"Made available under NASA sponsorship in the interest of early and wide dis-
semination of Earth Resources Survey Program information and without liability
for any use made thereof."

Progress Report

E 7.4 - 1 0.7 7 3.

CR14C126

Publications:

Publications presenting the analysis of aircraft and SKYLAB data (for-
warded earlier by separate mail) were presented at the University of Michi-
gan Remote Sensing of Environment Conference, held in Lansing, Michigan, in
April. Two papers were presented; one entitled "A Remote Sensing Study of
Pacific Hurricane AVA", by D. Ross, B. Au, W. Brown, and J. McFadden dealt
with the comparison of satellite and aircraft measurements of surface rough-
ness. The other, entitled "Multi-Frequency Radiometric Measurements of Foam
and a Mono-Molecular Slick", by B. Au, J. Kenney, L. Martin, and D. Ross,
dealt with aircraft measurements obtained during the pre-SKYLAB aircraft
program.

Efforts in Progress:

A further analysis of the AVA wind and wave data obtained by the aircraft
has been partially completed in collaboration with the University of Hamburg,
and a paper presenting these results is in preparation. The emphasis in this
paper is on the calculation of momentum transfer rates from the atmosphere to
the ocean by means of the observed wave spectra and wind speeds. Briefly, the
momentum flux to the wave spectra is related to the total wave energy, the
energy level of the higher frequency (short) waves, and the position of the
peak of the energy spectrum as follows:

$$C_{hf} = \frac{\tau_{hf}}{\rho_a U_{10}^2} = A \, \alpha^3 \, \bar{f}_m^{-2}$$

$$= B \, \tilde{E} \, \bar{f}_m^{10}$$

where A   = Const ≈ 4.2

B   = Const $\approx 1.05 \cdot 10^{12}$

τ_{hf} = Reynolds flux to the high frequency waves

ρ_a = Air density

α = Phillips constant as determined from the observed wave spectra

U_{10} = Surface wind speed at 10 meters

$\bar{f}_m = \dfrac{f_m U_{10}}{g}$ = non-dimensional peak frequency of the wave spectrum

$\tilde{E}$ = $g^2 E/U_{10}^4$ = non-dimensional total energy of the wave spectrum

Preliminary results of the calculation of this parameter for AVA data, when compared to other data at both lower and comparable (high) winds, suggest that there is an increased level of momentum flux for higher winds at all fetch lengths for growing seas. Thos AVA spectra, however, obtained near the periphery of the storm (where observed surface winds were 40 knots) show momentum transfer rates significantly less than one would expect for such high wind conditions. It is tentatively concluded that the presence of swell at a frequency very near the wind-wave peak frequency is responsible for this result. It should also be noted that visible estimates of white-cap coverage were also considerably lower than would be expected, supporting the previous calculations.

One implication of these results is that the energy level of the high frequency waves in the equilibrium region is not a unique function of the surface wind. To put it differently, scattering cross sections of the ocean surface may not be a unique function of the surface wind, but rather are reduced (for a given wind) in the presence of swell at frequencies nearby the peak frequency. The SKYLAB measurements of Hurricane AVA included both underdeveloped and decaying conditions in areas of high wind. It is not obvious, however, from the SKYLAB data in AVA that σ_0 measurements are particularly sensitive to the shape characteristics of the wave spectrum. This ray be due to improper corrections of σ_0 for aspect angle of viewing relative to the surface wind direction, attenuation, improper processing of the SKYLAB data itself, or the fact that the scattering cross sections saturate at wind speeds of 30 knots, or so. Analysis underway of AAFE RADSCAT and wave data obtained by the Houston aircraft program may resolve this discrepancy.

Additional efforts currently in progress concern reprocessing the wind data collected by the NOAA aircraft to remove small errors in wind direction and processing of aircraft-obtained microwave data. The final ground truth data package should be distributed within 30 days. Laser data from the Houston aircraft has recently been received for the SL4 period. Unfortunately, there appears to have been a problem with the record board of the JSC reproduce machine which duplicated the tapes, or the board was overdriven with too high voltage inputs. In either case, the tapes will have to be made again.

MULTI-FREQUENCY RADIOMETRIC MEASUREMENTS OF FOAM

AND A MONO-MOLECULAR SLICK

B. Au, J. Kenney, L. U. Martin

Naval Research Laboratory
Washington, D.C.

and

D. Ross

National Oceanic and Atmospheric Administration
Miami, Florida

ABSTRACT

Microwave radiometric measurements have
been made of both a surf-zone and of an ocean
region where small-scale roughness was sup-
pressed by an artificial mono-molecular slick.
The foam measurements show near identical foam
temperatures at 8.35 and 14.5 GHz, but large
variations at 1.4 GHz. The resultant maximum
foam emissivities at nadir range from 0.57 at
1.4 GHz to 0.84 at 14.5 GHz. The presence of
the mono-molecular slick on the ocean surface
has the same effect as a decrease in surface
roughness. For horizontal polarization, the
emission decreased below that of the surround-
ing ocean for all viewing angles. At vertical
polarization, the emission decreased below and
increased above a viewing angle of approximately
60 degrees. The change in temperature was ob-
served at both 8.35 and 14.5 GHz, being barely
detectable at 1.4 GHz.

---

1. INTRODUCTION

The dependence of the microwave brightness temperature on sea state and surface
wind fields is under active investigation and has led to the prospect of remotely
determining these parameters from a satellite on an all-weather basis. The useful-
ness of sea state and wind field data (in data scarce areas) would be of immense
value to both meteorologists and oceanographers alike. Two oceanographic effects
that play important roles in the dependence of the microwave signal on the sea sur-
face are small-scale wave structure and foam.

The dependence of the observed microwave signal on sea surface structure mani-
fests itself through the emission and reflection from dielectric media with all
scales of surface roughness. These include not only the relatively smooth wind wave
and swell much larger than the observing wavelength, but also the capillary and ultr
gravity waves present on the sea surface at low surface wind speeds. Current models
of the sea surface include roughness both larger and smaller than the observing wave
length, but the effect of small-scale structure on the radiometric signal has yet to
be experimentally verified.

Foam is a potentially more useful parameter to the remote sensing of the ocean
surface by microwave radiometry. Beyond an initial start velocity of 7 m/sec, foam
coverage increases with surface wind speed. The exact magnitude of the signal

increase depends on observing frequency, areal coverage of foam in the antenna beam and foam properties. Both the dependence of foam coverage with wind speed and the radiometric properties of foam are areas of active research. Of primary interest is the increase in temperature with frequency and the variation with viewing angle and polarization.

Experimental information about both of these phenomena has been obtained by the Naval Research Laboratory in a series of airborne multi-frequency radiometer measurements. In one set of observations, low altitude measurements were made of a surf-zone at a variety of viewing angles. In the other set, measurements were made of an ocean region in which the small-scale roughness had been suppressed by an artificial mono-molecular slick. This suppression enabled comparison to be made between an ocean surface having all scales of roughness present and one having just the large scale structure.

2. INSTRUMENTATION

The measurements in these experiments were made with a three frequency, non-scanning, airborne radiometer system mounted on a NOAA C-130 aircraft. The antennas all have identical seven-degree beamwidths and were mounted on a hydraulically controlled platform that allowed viewing angles from nadir out to 80 degrees to be obtained. The antennas at K_u(14.5GHz) and X-band(8.35GHz) were horn-fed dielectric lenses while the L-band(1.4GHz) antenna was a dipole-fed eight foot diameter paraboloid. Periodic calibration of the radiometers was provided by noise diodes couple into the reference arm of the radiometers. Simultaneous dual-polarization measurements were made at K_u- and X-band, while single polarization (either horizontal or vertical) was observed at L-band. Data were recorded both on analog strip-chart for instant monitoring purposes and also on magnetic tape for later digital processing. Sensitivity of the radiometers with a one second integration time was 0.21, 0.08 and 0.05 °K for L, X and K_u-bands respectively.

3. SLICK MEASUREMENTS

To determine the effect of small-scale roughness on the radiometric signal, one method is to suppress the small-scale waves in a specific area on the ocean surface. Although various types of oils damp small-scale waves, for sufficient oil thickness, oils have a radiometric effect of their own. This effect may overwhelm any change due to the damping of the small-scale structure. To eliminate this problem, oleyl alcohol was used for the experiment. It forms a mono-molecular slick on the ocean surface which is too thin to have a radiometric effect, yet damps out the capillary and ultra-gravity waves.

The oleyl alcohol was laid by the NOAA T-boat in the Atlantic Ocean about five miles from Miami, Florida. A total of nine passes along the length of the slick was made, with measurements being taken at angles from nadir out to 80 degrees. Based on laser geodilite data, the significant wave height was about 2.4 meters. Surface winds were 8 meters/sec, sufficient to produce some foam patches on the sea surface. Corresponding 35-mm photographs of the sea surface at a rate of one per second were used to confirm the areal extent of the slick.

The radiometer outputs as a function of time for a viewing angle of zero degrees are shown for horizontal polarization in Fig. 1 and vertical polarization in Fig. 2. The slick appears as a 2' K decrease in antenna temperature at both X- and K_u-bands and for both polarizations, with no detectable effect at L-band. The change in temperature with angle for both polarizations is summarized in Fig. 3 for K_u-band. The slick decreases the observed temperature for horizontal polarization at all angles, but produces an increase in temperature for vertical polarization near 80 degrees. Results obtained on 3 April 1973 under lighter sea state conditions are similar, but with a slight decrease in magnitude. The results for both days are summarized in Figs. 4 and 5, which show the temperature difference between polarizations due to the slick as a function of viewing angle. The difference between polarizations increases with increasing viewing angle and shows a slightly larger effect at K_u- than X-band. Surface roughness thus has little influence on the temperature change due to the slick until large viewing angles are obtained.

4. FOAM MEASUREMENTS

To investigate the radiometric properties of foam as a function of frequency and polarization, it is essential that the foam be identical in each case. This

Was accomplished in the field observations by making measurements simultaneously at three frequencies and at both horizontal and vertical polarization at X- and K_u-band By using identical seven degree beamwidths for all antennas, different foam coverage among beams are eliminated and comparison can then be made. To obtain good foam coverage and sufficiently thick foam, observations were conducted parallel to a surf. .one. The measurements were made from an altitude of 150 meters at angles from nadi· jut to 53 degrees.

Figures 6 and 7 show the radiometer output as a function of time for all of the radiometers at a viewing angle of 28 degrees. The wide variations in signal are due to both variations in foam properties and foam coverage. One can notice the correlation between the three frequencies and both polarizations, with only a difference in magnitude. To illustrate the response between the different frequencies, Figs. 8 and 9 show scatter diagrams of the temperature increase due to the foam at L- and K-bands plotted against the increase at K_u-band. The increase in all cases is the increase in brightness temperature above that from a specular surface. The linear relationship between X- and K_u-bands compared to the variability at L-band indicates that the foam was sufficiently thick to have the same response at the higher frequencies, but variable response at L-band.

The results for all viewing angles are summarized in Fig. 10, which shows the Maximum foam emissivity at K_u-band as a function of viewing angle for both polarizations. The results at X- and L-band are not shown as the X-band values are within 1% of those at K_u-band and those at L-band are similar in shape, only decreased in Magnitude. For comparison purposes, the empirical model as put forth by Stogryn is also shown for the same conditions as the experiment.

The maximum value of the experimental emissivity at nadir is 0.84, less than the theoretical maximum of 1.0 for a perfect emitter. The results for all of the frequencies are shown in Fig. 11, which shows the observed foam emissivities as a function of frequency for nadir viewing angle. The empirical model of Stogryn is again shown for comparison. One important feature is the increase in emissivity of foam from L- to X-band and the flatness of the curve from X- to K_u-band.

5. CONCLUSIONS

The absence of small-scale waves on the ocean surface changes the microwave emission at 8.35 and 14.5 GHz, and has a barely detectable effect at 1.4 GHz. At horizontal polarization, the change in emission is observed as a decrease in signal for all viewing angles. For vertical polarization, there is a decrease in emission for angles less than 60 degrees and an increase in signal beyond. The magnitude of the change in emission increases with increasing surface roughness, particularly for vertical polarization at large viewing angles. The measurements show that the sea surface becomes effectively smoother when the small-scale waves are damped, in that they have an exact opposite effect to an increase in surface roughness. Further experiments are required to determine whether the increase in emission from small-scale roughness is independent of the underlying large-scale roughness, or whether small-scale waves become important only after large-scale roughness is present. In any case, it is evident that small-scale roughness is important to the emission from the sea surface and must be included in any theoretical model.

The presence of foam on the sea surface is responsible for large increases in microwave emission at all of the frequencies investigated. The emission varies with areal coverage and foam properties, but is less at 1.4 GHz than at the higher frequencies. The variability at L-band is caused primarily by variations in foam depth, which are more important at the longer wavelengths. The emission from the foam is less than from a perfect emitter, but it is within 16% of that value at 14.5 GHz. For the thick foam of this experiment, the emissivity of foam increases gradually from 1.4 to 8.35 GHz, with neglible increase from 8.35 to 14.5 GHz. In general, the observed foam emissivities disagree with the empirical model of Stogryn, being up to 20 °K greater in magnitude than his model.

For the conditions of this experiment, where relatively thick foam was observed the frequency dependence occurs between L- and X-band. More experimental work is required to determine if this frequency dependence holds in general. It is unlikely that the emissivity of foam would have the same frequency dependence c. magnitude fc the foam patches and streaks on the sea surface during high wind conditions. For th thinner foam patches and streaks, the change in emissivity would most likely occur at higher frequencies.
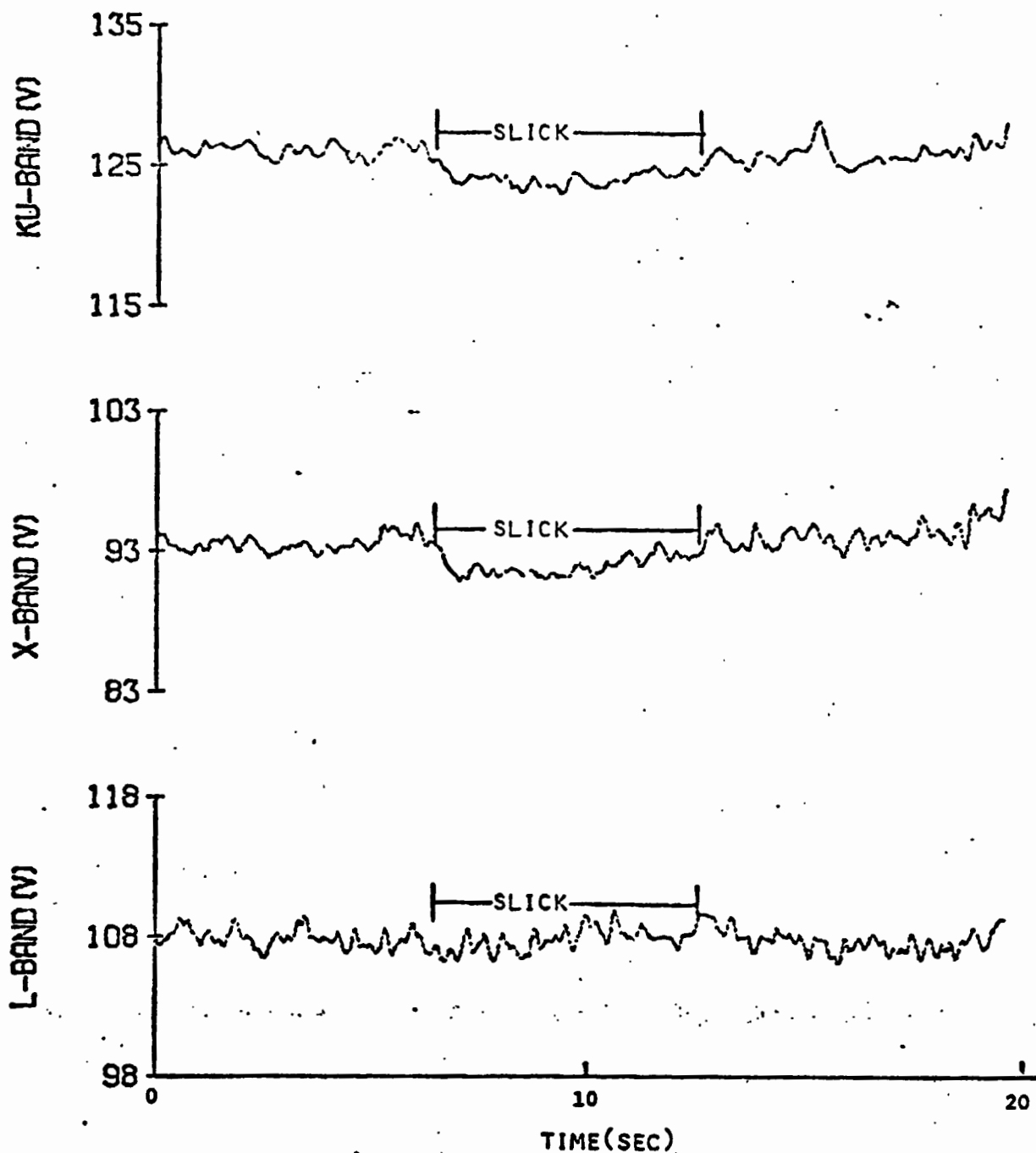
FIGURE 2: ANTENNA TEMPERATURES ALONG SLICK. Vertical
polarization, Frequencies = 1.4, 8.35 and 14.5 GHz,
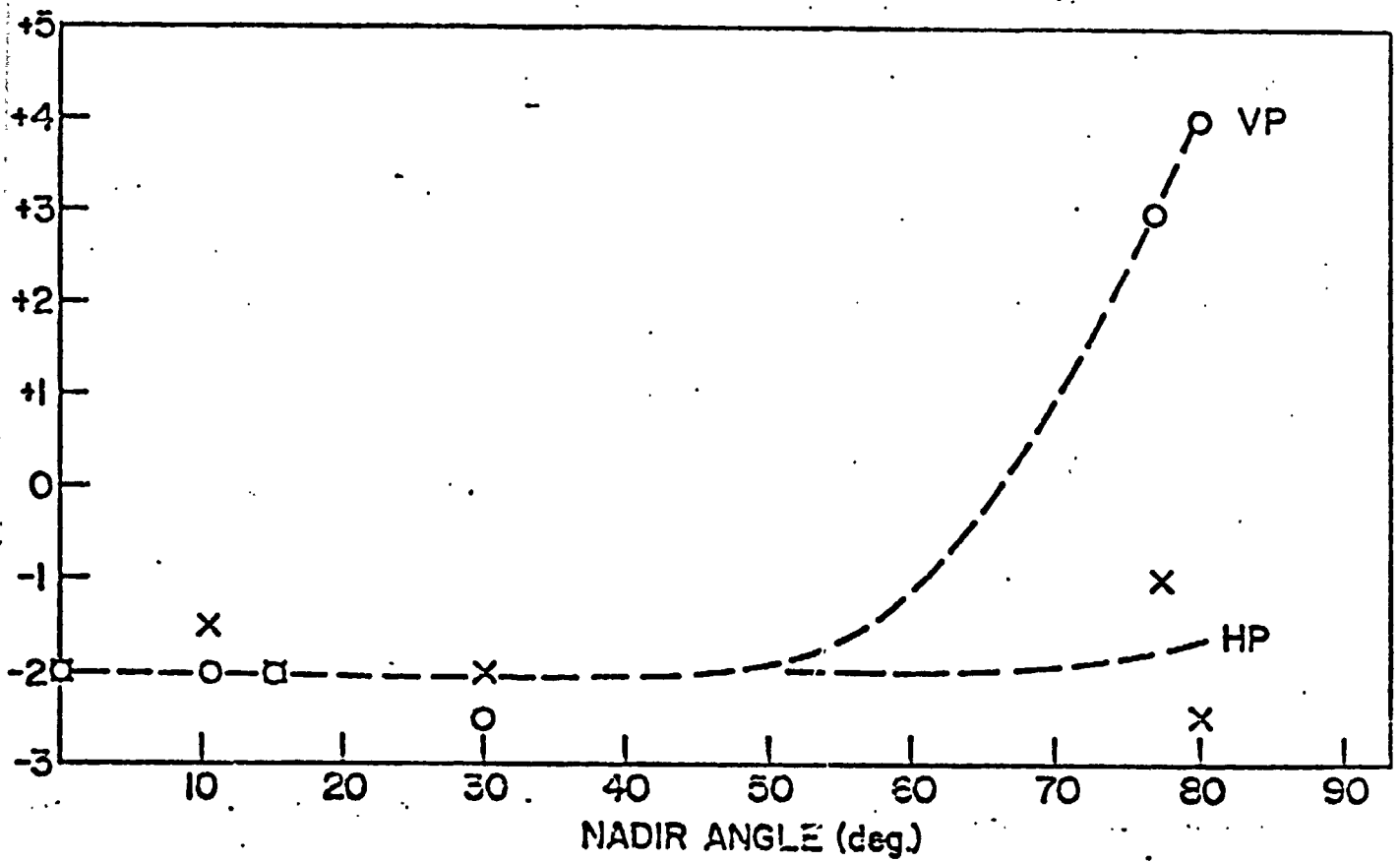Viewing angle = 0°, 11 April 1973.

FIGURE 3. ANTENNA TEMPERATURE CHANGE DUE TO SLICK VERSUS VIEWING ANGLE. Horizontal and vertical polarization, Frequency = 14.5 GHz, 11 April 1973.
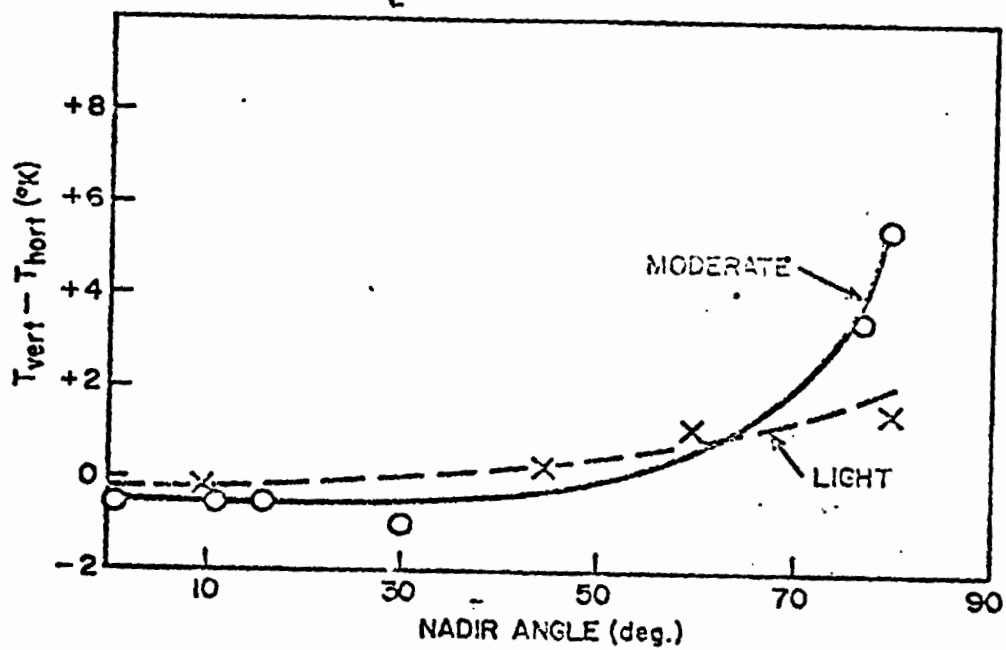
FIGURE 4. ANTENNA TEMPERATURE DIFFERENCE BETWEEN POLARIZATIONS VERSUS VIEWING ANGLE. Light and moderate surface roughness, Frequency = 8.35 GHz, 3 and 11 April 1973.
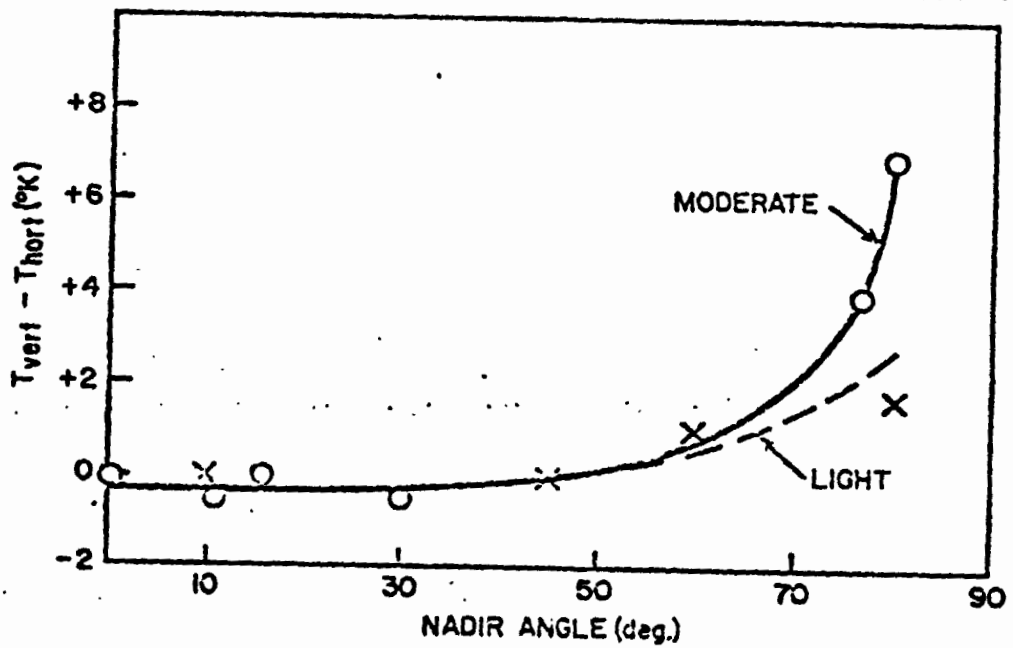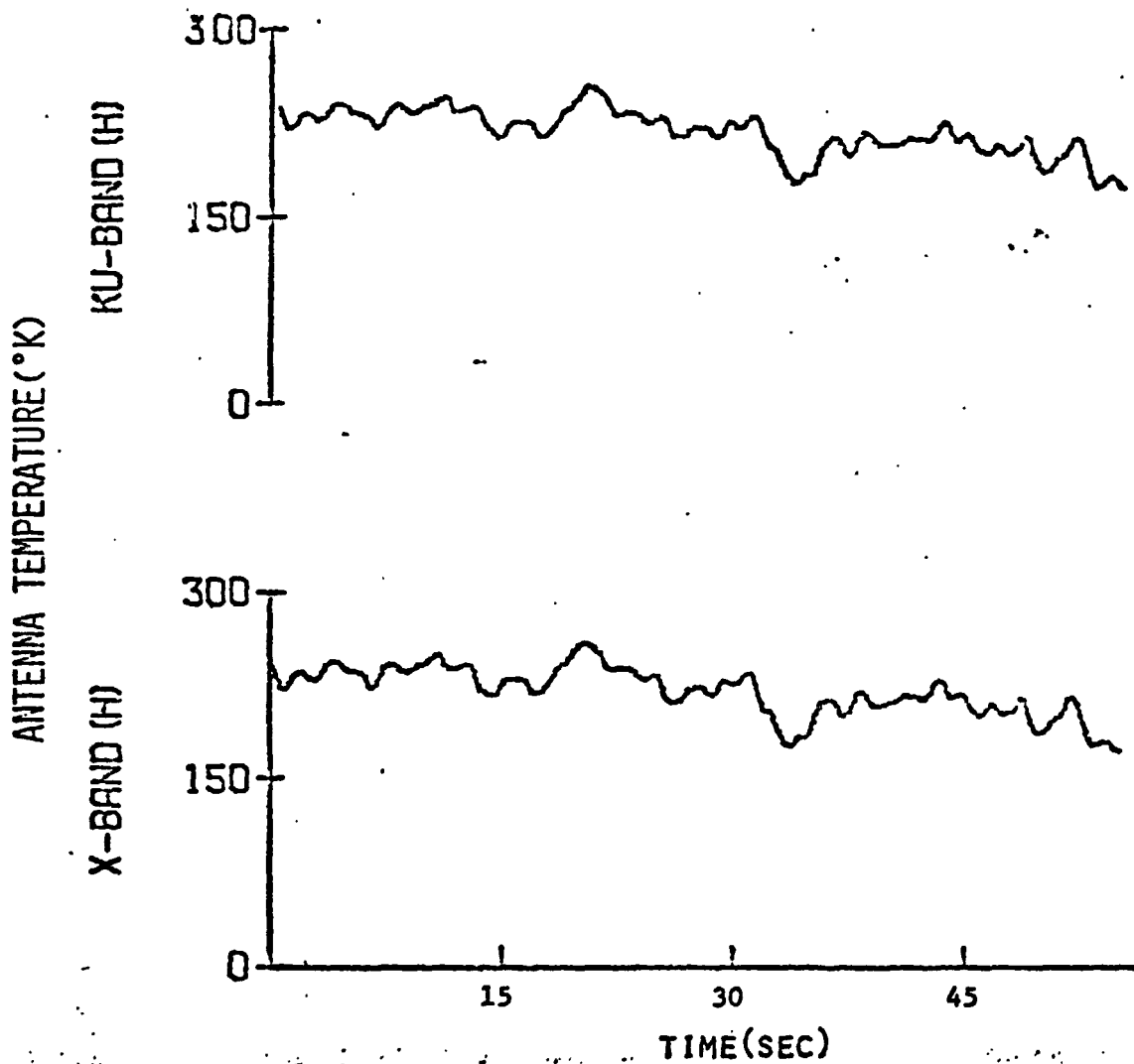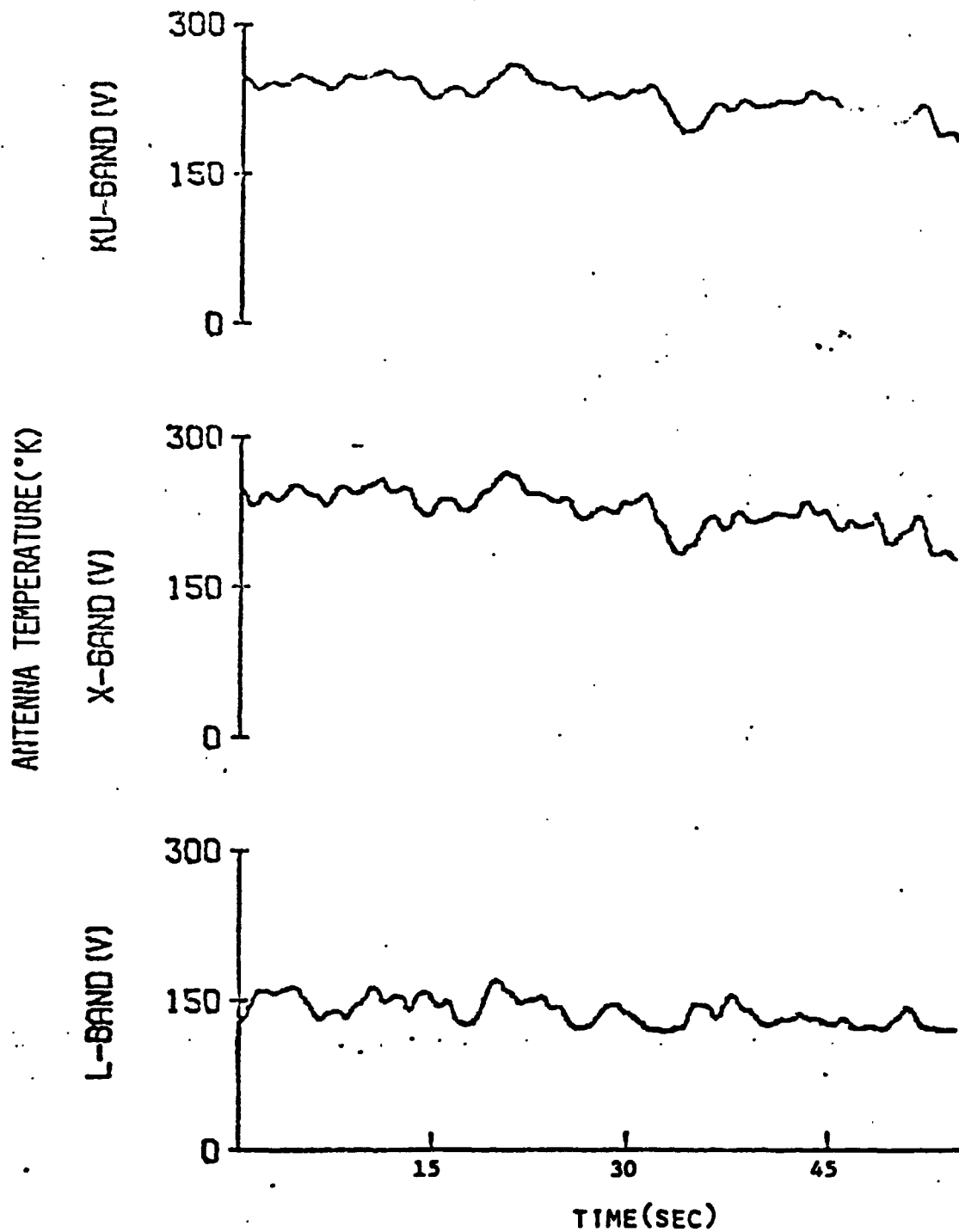

FIGURE 5. ANTENNA TEMPERATURE DIFFERENCE BETWEEN POLARIZATIONS VERSUS VIEWING ANGLE. Light and moderate surface roughness, Frequency = 14.5 GHz, 3 and 11 April 1973.

FIGURE 6. ANTENNA TEMPERATURES ALONG SURF-ZONE.
Horizontal polarization, Frequencies = 8.35 and
14.5 GHz, Viewing angle = 28°, 6 June 1973.

FIGURE 7. ANTENNA TEMPERATURES ALONG SURF-ZONE.
Vertical polarization, Frequencies = 1.4, 8.35
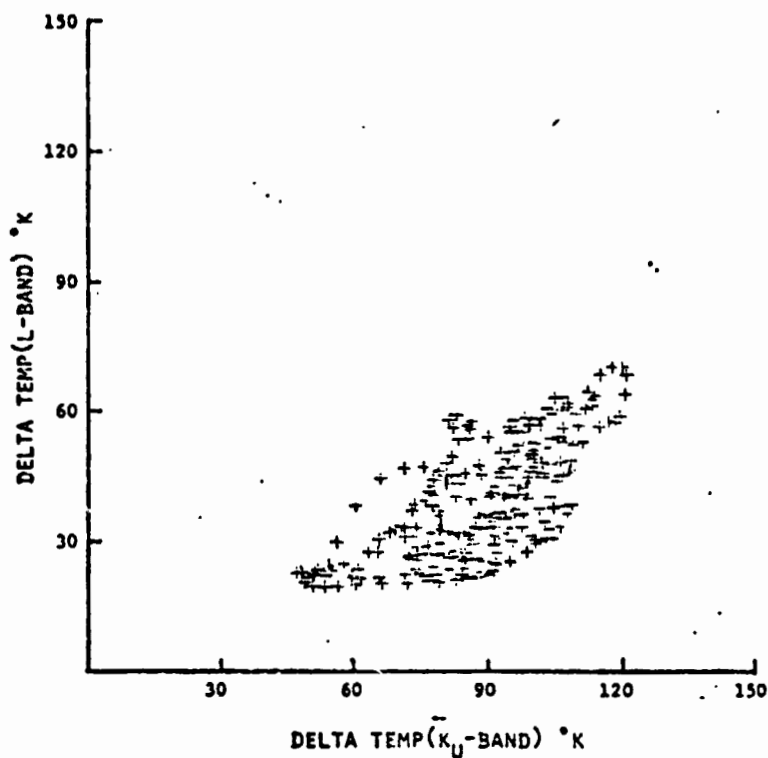and 14.5 GHz, Viewing angle = 28°, 6 June 1973.

FIGURE 8. SCATTER DIAGRAM OF TEMPERATURE
INCREASE DUE TO FOAM AT L- AND K_u-BANDS.
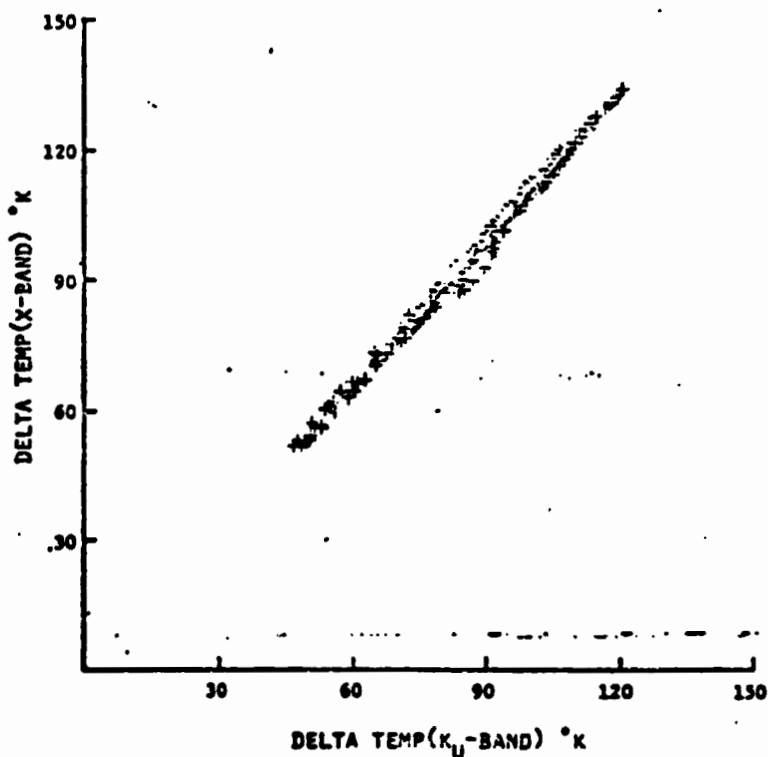Vertical polarization, Viewing angle =
28°, 6 June 1973.

FIGURE 9. SCATTER DIAGRAM OF TEMPERATURE
INCREASE DUE TO FOAM AT X- AND K_u-BANDS.
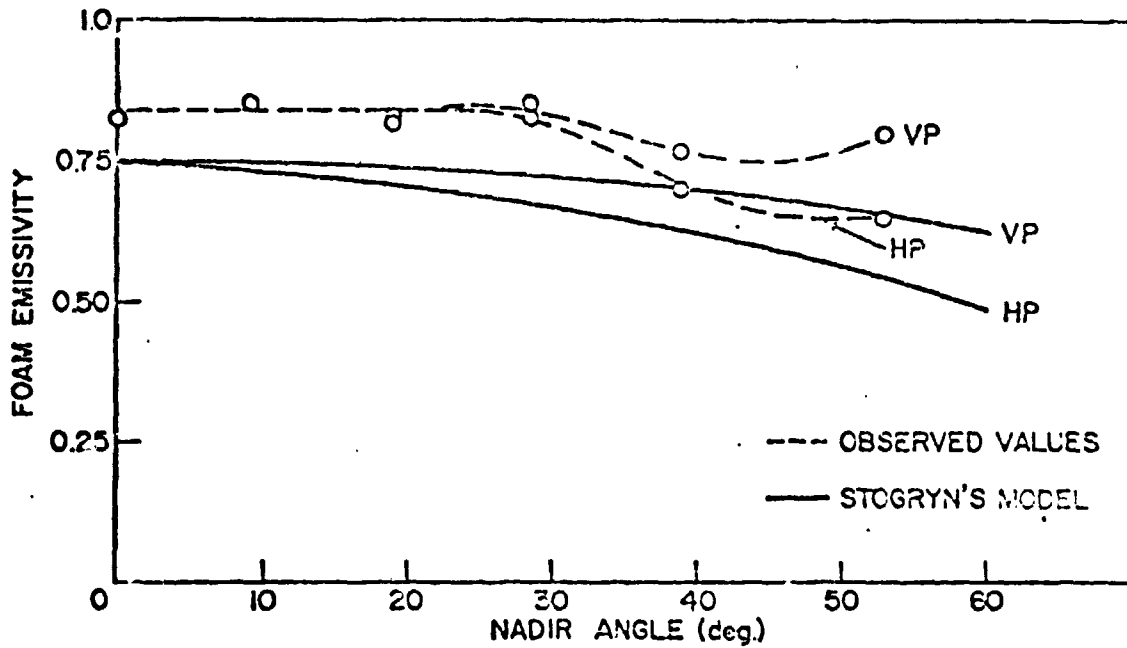Vertical polarization, Viewing angle =

FIGURE 10. EMISSIVITY OF FOAM VERSUS VIEWING ANGLE. Horizontal and vertical polarization, Frequency = 14.5 GHz, 6 June 1973.
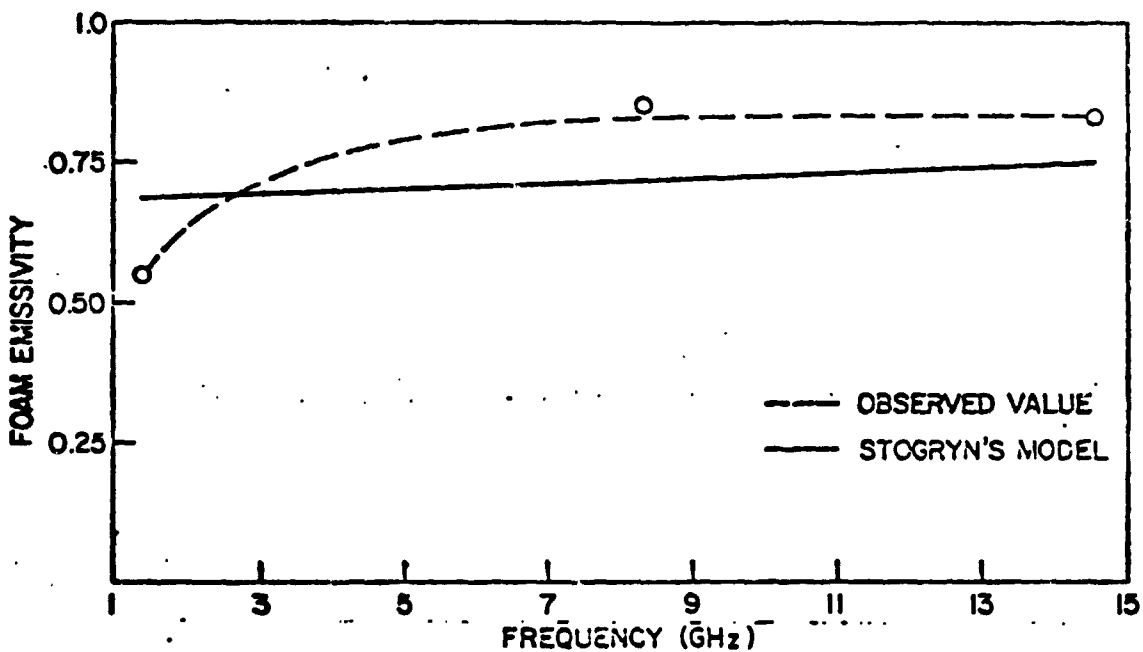

FIGURE 11. EMISSIVITY OF FOAM VERSUS FREQUENCY. Viewing angle = 0°, 6 June 1973.

A REMOTE SENSING STUDY OF PACIFIC HURRICANE AVA

D. Ross

National Oceanic and Atmospheric Administration
Miami, Florida

B. Au

Naval Research Laboratory
Washington, D. C.

W. Brown

Jet Propulsion Laboratory
Pasadena, California

J. McFadden

National Oceanic and Atmospheric Administration
Miami, Florida

ABSTRACT

Aircraft, SKYLAB, NOAA-2, ATS-3, and NIMBUS-5 recently obtained a variety of measurements of Pacific Hurricane AVA. These measurements are unusually broad in scope and include satellite observed passive microwave emissivities at 13.9 + 19.5 GHz, active microwave scattering cross-sections at 13.9 GHz, and near infrared and visible images. Essentially simultaneous aircraft measurements of wind speed, waves, whitecaps, 1.4 and 13-15 GHz passive microwave emissivities, 1.4 GHz active microwave images, sea surface temperatures, pressure fields, and aerosol size distributions were also obtained. A brief description of sensors and platforms is presented along with some in-depth details of results obtained. These results confirm the sensitivity of microwave emissivity to foam and liquid water in the atmosphere. Wave measurements from the aircraft show significant differences in the shape of the energy spectrum when compared to other fetch-limited spectra. Whereas fetch-limited spectra are sharply peaked, the hurricane spectra remote from the eye are broad, indicating the presence of swell and increased energy transfer within the spectrum due possibly to non-linear interactions, while those near the eye are sharply peaked.

The SKYLAB RADSCAT, operating at 13.9 GHz in a cross-track mode, obtained microwave measurements of a portion of the storm in both the active and the passive mode. Preliminary results show that the scattering cross-sections increase when viewing the hurricane despite an expected attenuation due to rain. Passive measurements increase as expected and are in general agreement with NIMBUS-5 measurements at 19.5 GHz.

Aircraft measurements of microwave brightness temperatures at L band show an increase which is

c

largely due to foam and whitecaps while those at X
and KU band are contaminated by rain. Active co-
herent L-band radar images of swell produced by the
hurricane were obtained enroute to the storm. These
images indicate a strong interaction takes place be-
tween long and short gravity waves.

Flight level wind speeds were obtained by means
of an inertial navigation system and represent a sig-
nificant increase in accuracy from past measurements
of hurricane winds. Maximum winds encountered in
the eye wall measured 137 knots, the highest ever
for a Pacific hurricane, which had a record low cen-
tral pressure of 914 mb.

The use of extensive and coordinated satellite
and aircraft measurements has provided an unprece-
dented opportunity to study the dynamics of a hurri-
cane.

.1. INTRODUCTION

The development and application of remote sensing techniques to the study of
man's environment has increased considerably in recent years. Perhaps the greatest
return on monies invested in this area has been in use of satellites in observing
and predicting weather. One aspect of weather phenomena which is currently being
studied in great detail is tropical cyclones. A tropical cyclone is an intense
vortex of high winds and large moisture concentrations which can have a devastating
effect on man as they pass from water to land accompanied by high wind forces, in-
ordinately high water (surge) levels, and large amounts of rain. Because cyclones
are generally born in remote ocean areas, they have remained a little understood
phenomena. In recent years, however, aircraft have been used to study many aspects
of the storms by means of a variety of in-situ measurements. More recently, sate_-
lites equipped with imaging systems have been of great utility in detecting the
birth of cyclones and predicting the path they are most likely to follow during
their lifetime.

This paper describes a number of measurements of some unique aspects of a cy-
clone obtained from aircraft and a variety of spacecraft and represents an unprece-
dented opportunity to evaluate the capability of remote sensing instrumentation to
contribute to the study of such phenomena.

2. BACKGROUND

The NASA SKYLAB experimental satellite was the catalyst needed to gel this ex-
periment. Intended as a means of evaluating the Radar-Radiometer sensor packages
aboard SKYLAB, an aircraft program was initiated to fly beneath the SKYLAB and mea-
sure an extensive number of environmental parameters which might affect the signa-
ture of the earth viewing satellite sensors. One of the aircraft involved was a
National Oceanic and Atmospheric Administration (NOAA) C130 Hercules normally
equipped to study hurricanes and other weather-oriented phenomena. For the SKYLAB
program, a number of additional sensors were installed and are shown in Table I
along with the parameter intended to be studied and expected accuracy. Figure 1
shows the NOAA aircraft with passive microwave radiometers extended out the rear
cargo door.

As the NOAA SKYLAB underflight program was getting underway, the first Pacific
Hurricane of the season was forming and was named AVA, (Figure 2). As one of the
objectives of the SKYLAB program was to observe hurricanes, a data gathering pass
was planned for 6 June 1973, using the SL 193 Radar-Radiometer in the solar inertial
scanning mode. Unfortunately, a more extensive look at the hurricane with other
SKYLAB sensors could not be arranged because of conflicting priorities. Indeed, the
NASA system was literally turned upside down in order to schedule this limited pass.

3. AIRCRAFT MEASUREMENTS

The NOAA C130 deployed to Acapulco the morning of 6 June, refueled and commenced its flight into the storm at 2107Z. Figure 3 shows the track of the aircraft along with isolines of flight level (500 ft.) winds measured with a Litton LTN-51 inertial system using the true airspeed output from a Kollsman differential pressure transducer. As a result of a measurement of an extraordinarily low central pressure of 915 mb obtained by an Air Force Reconnaissance aircraft approximately three hours prior to our entry into the storm, it was decided a low level (500 ft.) penetration into the eye would be unwise. The portion of the track shown in Figure 3 from 2156 to 2315 was therefore flown at 10,000 feet. Low level (500 ft.) measurements of wind speed and direction, wave heights, whitecap densities, and microwave emissivities were obtained during the period 2107-2156, and again from 2325 to 2356. Microwave measurements, which require the cargo door to be open with extended radiometers, were not taken during the latter time period because of the reduced safety factor associated with high turbulence in conjunction with open cargo doors.

Figure 4 is an example of laser altimeter profiles of waves in an area of 65 knot flight level winds. Figure 5c shows the spectra of this segment, mapped to fixed coordinates, along with a spectra of high waves measured in the North Sea (Ross, et al., 1970). Also shown are spectra (Panel a, b) obtained at other regions within the storm plotted together with spectra of the same total energy obtained in the N-Sea and the North Atlantic. There are some significant differences between these sets of spectra. Those obtained near the eye (Fig. 5b, c) are sharply peaked and agree well with the N-Sea spectra which are severely fetch limited. The third spectrum was obtained approximately 110 nautical miles from the eye and shows considerably more low frequency energy than the North Atlantic spectrum which was essentially fully developed. In addition, this spectrum shows a reduced level of energy on the high frequency side of the peak. We attribute this difference to non-linear interactions between the high frequencies and swell of frequencies near the peak which results in a broadening of the hurricane spectrum. Figure 6 shows the variation of wind speed and significant wave height with radial distance from the eye. The dashed line shows expected surface (20 meter) winds assuming a logarithmic variation in wind between the surface and flight altitude (Cardone, 1969). The significant wave height is known to vary as the square of the wind speed for fully developed seas. It can be seen in this figure that this relationship does not hold in a hurricane because of the fetch and duration limited character of the hurricane wind field.

Observations of microwave brightness temperature were obtained during the period 2107-2147. The data at the higher microwave frequencies are strongly affected by the presence of rain as one-minute average values at vertical incidence vary inconsistently from 130° to 145°, and 140° to 200° for X and KU Band respectively. Brightness temperature vs. incidence angle for this segment at L-Band is shown in Figure 7 along with data for a low wind condition obtained 11 June. It can be seen that there is a systematic increase in brightness temperatures of about 4°K at all incidence angles. Inspection of simultaneous vertical photography reveals little thin foam streaking presumably because of the swell content of the seaway and the percentage of whitecap coverage is approximately 10 percent. Based on the results of Au, et al. (1974), presented elsewhere in this symposium, we attribute this increase to the whitecap (foam) coverage. Thus, a sensitivity of $.4^\circ$K/% whitecap coverage is obtained.

Enroute to the storm, coherent side-looking radar operating at a frequency of 1.35 GHz ($\lambda = 25$ cm) was used to obtain surface imagery. A series of wave-like patterns is apparent in this imagery which appears to be a combination of locally generated wind waves mixed with swell coming from the hurricane. This imagery, together with a vertical photograph obtained simultaneously, was digitized and subjected to two-dimensional Fourier analysis. Figure 8 shows the optical image of the two-dimensional Fourier transform at the top, along with a densitometer trace obtained along the axis of the principal direction (lower left, and center). Also shown is a composite hindcast wave spectrum constructed by using the wave spectra obtained at 2147Z along with a spectrum obtained in the Atlantic Ocean for a wind speed of approximately 22 knots. Surface winds at the time of this image were visually estimated to be 20 knots, which was substantiated by sun glint analysis of ATS-3 Satellite imagery (Strong, 1973). The position of the laser wave measurements and of the hurricane relative to the radar imagery is shown in the inset in

the upper right corner of the figure. Good agreement between the wave lengths of the principal wave components can be seen. That the radar is imaging the waves is evident; not so evident is the scattering mechanism which allows detection of waves longer than the backscattering Bragg waves (Crombie, 1955). It has been demonstrated in several laboratory and field experiments (cf. Shemdin, et al., 1972, Mitsuyasu (1971)) that presence of a swell in a wind sea will reduce the amplitude of the wind-wave energy peak by an amount which is dependent upon the energy and frequency separation of the swell. Longuet-Higgins (1969) describes this interaction which results in shorter waves peaking near the crest of the longer wave as it passes by. The long waves thus modulate the Bragg waves which, in turn, modulate the return of the radar energy resulting in an image of the longer waves. Since more than one long wave component is seen in the image, it has been suggested (Stilwell, 1974) that this modulation is accomplished by interaction between all waves longer than the Bragg waves. The radar imagery therefore may contain useful amplitude as well as wave length and direction information if the transfer function for the former can be established. Unfortunately, the radar power supply gave out shortly after this segment was completed so that no imagery of the local hurricane wave field was obtained during the eye penetration.

4. SATELLITE RESULTS

Imagery and microwave data from a variety of satellites were obtained of the hurricane in various stages of development. A summary of these satellite studies is shown in Table II. Figure 9 is a composite of the imagery showing the track of SKYLAB as it passed near the storm. Unfortunately, the storm was moving rather fast, and although the SKYLAB antenna scanned to 50° incidence angle, only a small portion of data was obtained in the high wind periphery of the storm. This data, along with NIMBUS 19.5 GHz measurements of the same portion of the storm, are shown in Figure 9 for the incidence angles of 45° to 52.5°. Also shown are rainfall rates inferred from the 19.5 GHz NIMBUS-5 radiometer (Wilheit, 1974). .

The purpose of the S 193 Radar-Radiometer is to infer surface wind fields from measurements of the microwave backscatter. The passive portion of the instrument is intended to provide a basis for correcting the return radar cross-section (σ_o) due to attentuation by liquid water. The inference of surface wind speed is further complicated because the amplitude of the backscattered component is sensitive to the relative direction of the wind vector. Jones (1974), from data obtained with an aircraft system at vertical polarization, reports a difference of about 5 db between the upwind and cross-wind directions for a wind speed of 14 m/s and incidence angle of 40°, vertical polarization. The up-downwind asymmetry he observed of 1-2 db is further evidence of short wave modulation by longer waves. Estimates of wind direction along the footprint were made as previously described and resulted in positive corrections of 2-4 db. A backscattered component due to rainfall is not accounted for in the data which are summarized in Table III.

It can be seen from panel a of Figure 10 that if a correction were applied to σ^o values, due to rain attentuation, that the σ^o for both polarizations would increase with increasing wind speed between 1857:15 and 1858:00. Neglecting the value at 1858:16, σ^o would then decrease at 1858:31, following the decreasing trend in surface wind. At the 45° incidence angle (panel b), rainfall rates were markedly reduced and σ^o qualitatively agrees with trends in the wind speed. $\sigma_{VV}{}^o$, in both cases, has been corrected for wind direction while no such correction has been applied to $\sigma_{HH}{}^o$. As with the coherent radar images, the σ^o is a measure of the energy content of resonant Bragg waves - near capillary, or centimeter, wavelengths in the case of the S 193 radar. Phillips (1966) using dimensional arguments shows that the high frequency end ($f_i > f_m$)* of the gravity wave spectrum should reach a maximum, or equilibrium, value. Increased energy transfer into this spectral region would simply result in increased energy loss through wave breaking. Pierson and Stacy (1973) suggest three forms for the behavior of the high frequency end of the spectrum, including the ultra-gravity and capillary regions, which are wind speed dependent and result in increased wave energy levels for all increasing winds. Hasselmann, et al. (1973), show that the Phillips equilibrium constant decreases with increasing fetch indicating long wave-short wave interaction is important in the behavior of the high frequency tail of the spectrum.

---

*f_m is the frequency at which the peak energy occurs.

From the observations of SKYLAB measurements obtained in hurricane AVA, it is tempting to attribute the observed σ^o variations to corresponding variations in energy level of wind speed dependent Bragg waves. On the basis of this limited data set, the considerable potential for errors associated with the corrections required for attenuation, relative wind direction, and backscatter due to rain, and an unknown sensitivity of σ^o at high wind speeds, we reject this step at this particular time. A final conclusion must await additional data obtained for high sea states during SL4 and a better estimate of azimuth dependence of σ_o for different wind speeds and both polarizations.

5. CONCLUSIONS

It can be concluded from this data set that the use of remote sensors could be a useful tool in the monitoring and study of tropical cyclones. The potential for such sensors listed by observational category is as follows:

1. **Active microwave** - Both cross-sectional as well as imaging microwave systems can be used to map aspects of the wave field of a hurricane. High frequency systems, such as the SKYLAB RADSCAT, may have reduced utility in areas of heavy rain, while low frequency imaging systems will be limited primarily by the required high data rates.

2. **Passive microwave** - Aircraft and satellite measurements at 1.4, 8.35, 14, and 19.5 GHz show the higher frequencies to be capable of determining liquid moisture budget while the lower frequencies could be useful for determining the atmosphere-ocean energy exchange budget because of a sensitivity to energy loss occurring through the wave spectrum. However, because of diminished sensitivity at 1.4 GHz, a frequency somewhat higher, but less than 6 GHz, would be more appropriate.

3. **Visible:**

   a. **Satellites** - Visible region imagery has been extremely useful in positioning the hurricane, calculating its forward velocity, and estimating the degree of asymmetry of the hurricane.

   b. **Coherent** - Red laser light can be used with good results from low aircraft altitudes to profile surface waves despite heavy rain and spray, and the wave measurements can be used to bound the role of momentum transport to the ocean.

   c. **Photographic** - Observations of whitecap density, which is related to momentum transfer and the wave spectrum, can be obtained. Thin foam streak direction relative to the eye of the hurricane could give an estimate of inflow angle of the surface winds.

REFERENCES

Au, B., J. Kenney, L. U. Martin, D. B. Ross, Multi-frequency radiometric measurements of foam and a mono-molecular slick, Proceedings of the Symposium on Remote Sensing of Environment, Willow Run Laboratories, Ann Arbor, Michigan, 1974.

Cardone, V. J., Specification of the wind field distribution in the marine boundary layer for wave forecasting, Rep. TR 69-1, Geophys. Sci. Lab., New York Univ., New York, December, 1969.

Crombie, D. D., Doppler spectrum of sea-echo at 13.56 mc/s, Nature, 175, 681-682, 1955.

Hasselmann, et al., Measurements of wind-wave growth and swell decay during the Joint North Sea Wave Project (JONSWAP), Deut. Hydrogr. Z., Deutsches Hydrographisches Institut, Hamburg, FRG, 1973.

Jones, W. Linwood, Personal communication, 1974.

Longuet-Higgins, M. S., A nonlinear mechanism for the generation of sea waves, Proc. Roy. Soc. A., 311, 371-389, 1969.

Mitsuyasu, H., R. Nakayama, T. Komori, Observations of wind and waves in Hakata Bay, Rep. Research Inst. Appl. Mech., Kyushu Univ., 19, 37-74, 1971.

Phillips, O. M., The dynamics of the upper ocean, 261 pp., Cambridge University Press, London, 1966.

Ross, D. B., and V. J. Cardone, Laser observations of wave growth and foam density for fetch-limited 17-25 m/s winds, IEEE Trans. Geosci. Electron., GE-8(4), 326-336, 1970.

Shemdin, O. H., R. J. Lai, A. Reece, and G. Tober, Laboratory investigations of white-caps, spray, and capillary waves, Tech. Report No. 11, Coastal and Oceanographic Engineering Laboratory, Univ. of Florida, Gainesville, Florida, 1972.

Strong, A., Personal communication, 1973.

Stilwell, D., Personal communication, 1974.

Wilheit, T., Personal communication, 1974.

TABLE I. NOAA C130 AIRCRAFT INSTRUMENTATION

Parameter	Instrument	Accuracy
Wind Speed/Direction	LTN-51 Inertial Navigation System	$\pm$ 2.0 kts
Sea Surface Temperature	Barnes PRT-5	$\pm$ 1.0°C
Microwave Emissivity	1.4, 8.5, 14 GHz Radiometers	$\pm$ 1.0°K
Wave Heights and Lengths	Laser Altimeter	$\pm$ 1% or 3"
Wave Length and Direction	Coherent Radar 1.35 GHz	$\pm$ 10%
White Caps and Foam	35 mm Vertical Camera	$\pm$ 20% of Observation
Liquid Water Content	Johnson Williams Hot-Wire	$\pm$ 15%

TABLE II. SUMMARY OF SATELLITES USED TO STUDY HURRICANE AVA

Satellite	Imagery Type	Microwave Data	Use
1. ATS	Visible	—	Positioning, Cloud cover
2. NIMBUS-5	Microwave	19.5 GHz HH, VV	Positioning, Rainfall rate
3. NOAA-2	Visible	—	Positioning, Asymmetry
	Infrared	—	Cloud Cover
4. SKYLAB	Photography	13.5 GHz HH, VV	Surface Winds
		HV, VH	Rainfall Distributions
5. DPP	Visible		Positioning, Cloud cover, Asymmetry
	Infrared		Cloud Heights

TABLE III. SUMMARY OF SATELLITE OBSERVATIONS

SKYLAB Time	NIMBUS-5 19.5 GHz T_{BH} (°K)	Rain-fall (mm/hr)	S193 T_{HH} (°K)	S193 T_{VV} (°K)	S193$_0$ σ_{VV} (db)	S193$_0$ σ_{HH} (db)	$\bar{U}_{20}$ (kts)	θ_U (Deg.)	Rela-tive Azi-muth (Deg.)	$\sigma_{VV}°$ Cor-rec-tion (db)	S193 Inci-dence Angle (Deg.)
1857:15	170	2	121	173	-14	-19	36	90	150	+2	52.5
1857:30	170	2	124	174	-14	-20	42	90	150	+2	52.5
1857:45	193	25	145	188	-13	-16	48	120	120	+4	52.5
1858:00	193	25	152	189	-14	-15	40	160	80	+3	52.5
1858:16	200	50	216	233	-13	-13	39	160	80	+3	52.5
1858:31	180	5	135	185	-17	-19	32	160	80	+3	52.5
1857:18	170	2	122	161	-14	-17	32	90	150	+2	45.0
1857:34	170	2	122	161	-14.5	-19	36	90	150	+2	45.0
1857:49	170	2	140	175	-15	-16	36	110	130	+3	45.0
1858:04	175	3	136	171	-13	-16	37	140	100	+5	45.0
1858:20	182	6	128	165	-14.5	-18	36	120	120	+4	45.0
1858:35	180	5	132	169	-18.5	-21	28	100	100	+5	45.0
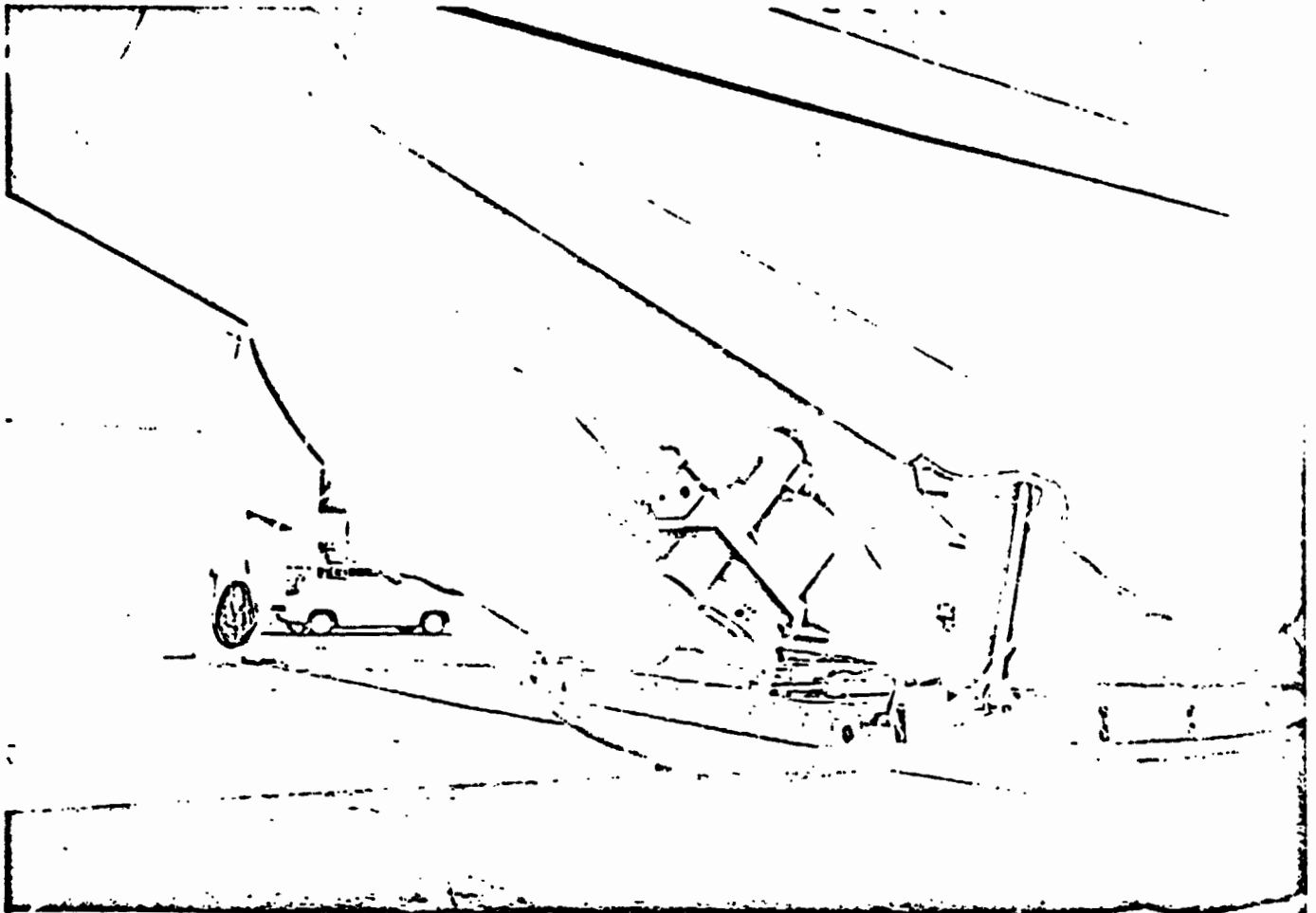
FIGURE 1. NOAA RESEARCH FLIGHT FACILITY C130 AIRCRAFT SHOWING 1.4 GHZ
PASSIVE RADIOMETER IN THE VERTICAL INCIDENCE FLIGHT POSITION.

Fig 2

FIGURE 2. NOAA-2 VISIBLE REGION VIEW OF
PACIFIC HURRICANE AVA ON 6 JUNE 1973.
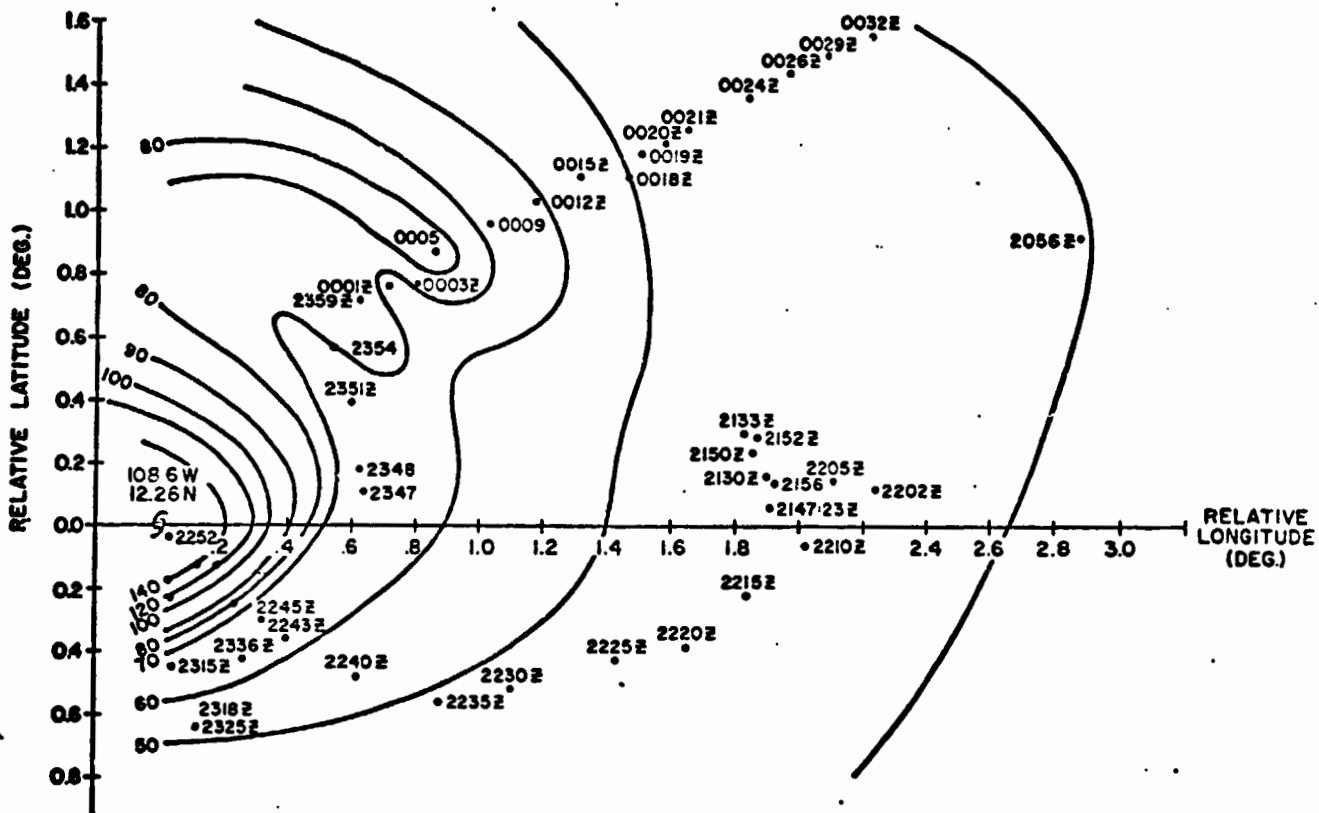
FIGURE 3. FLIGHT TRACK OF NOAA C130 AND ISOLINES OF 150 M
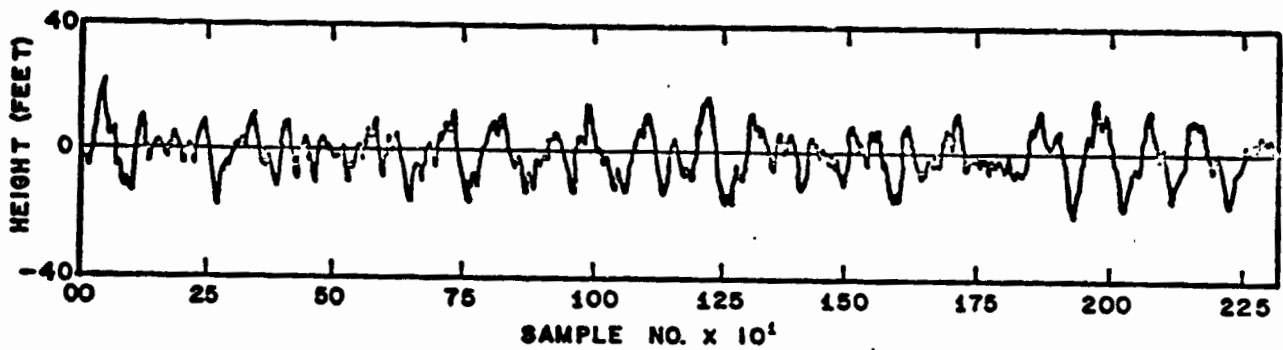WIND SPEEDS IN REAR QUADRANTS OF PACIFIC HURRICANE AVA.

FIGURE 4. LASER MEASUREMENTS OF SURFACE WAVE CONDITIONS NEAR THE CENTER OF PACIFIC HURRICANE AVA. Flight level winds averaged for 1 minute were 65 kts.
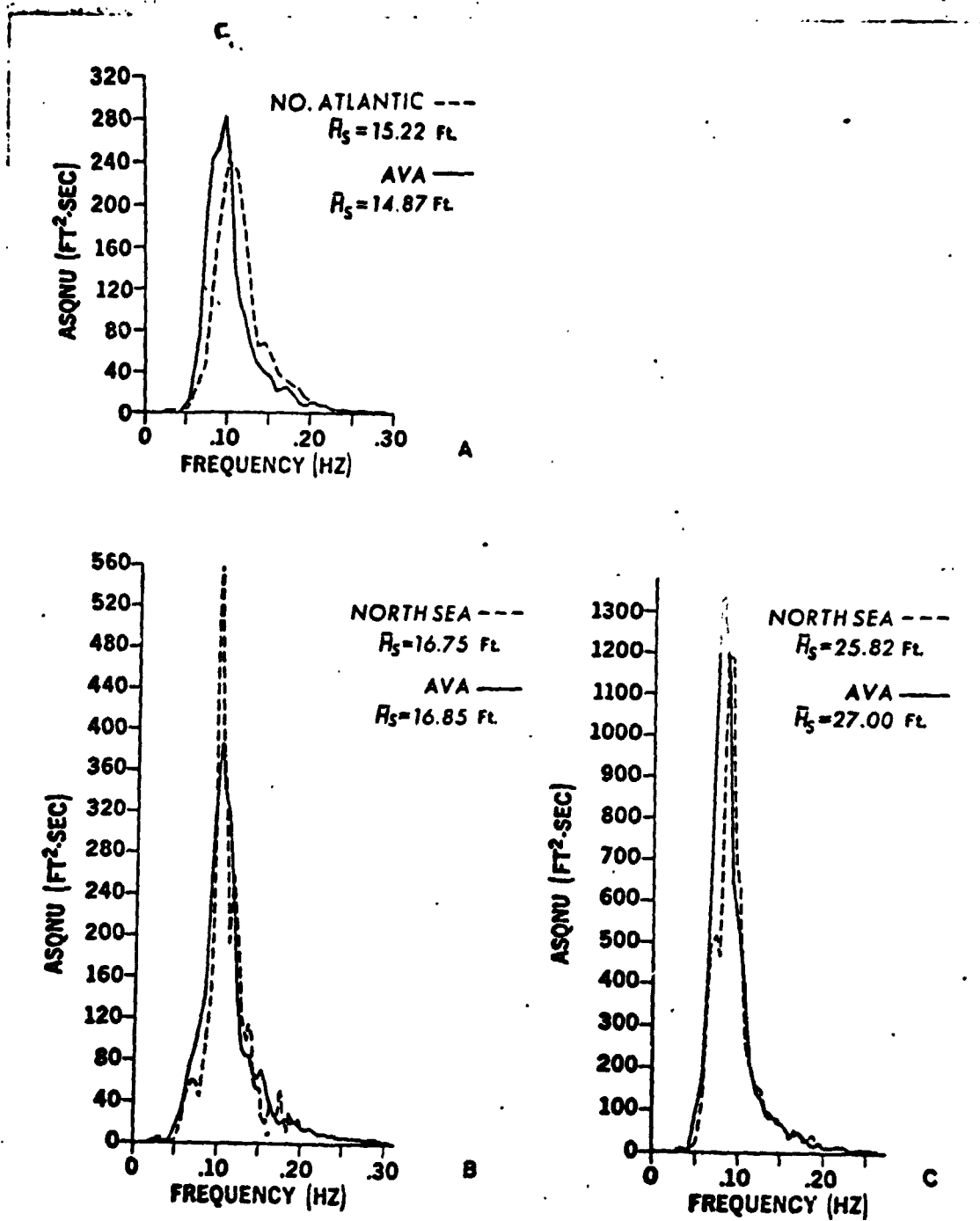
FIGURE 5. HURRICANE AVA WAVE SPECTRA COMPARED TO OTHER
SPECTRA OF SIMILAR ENERGY CONTENT AND WIND SPEEDS.

F165
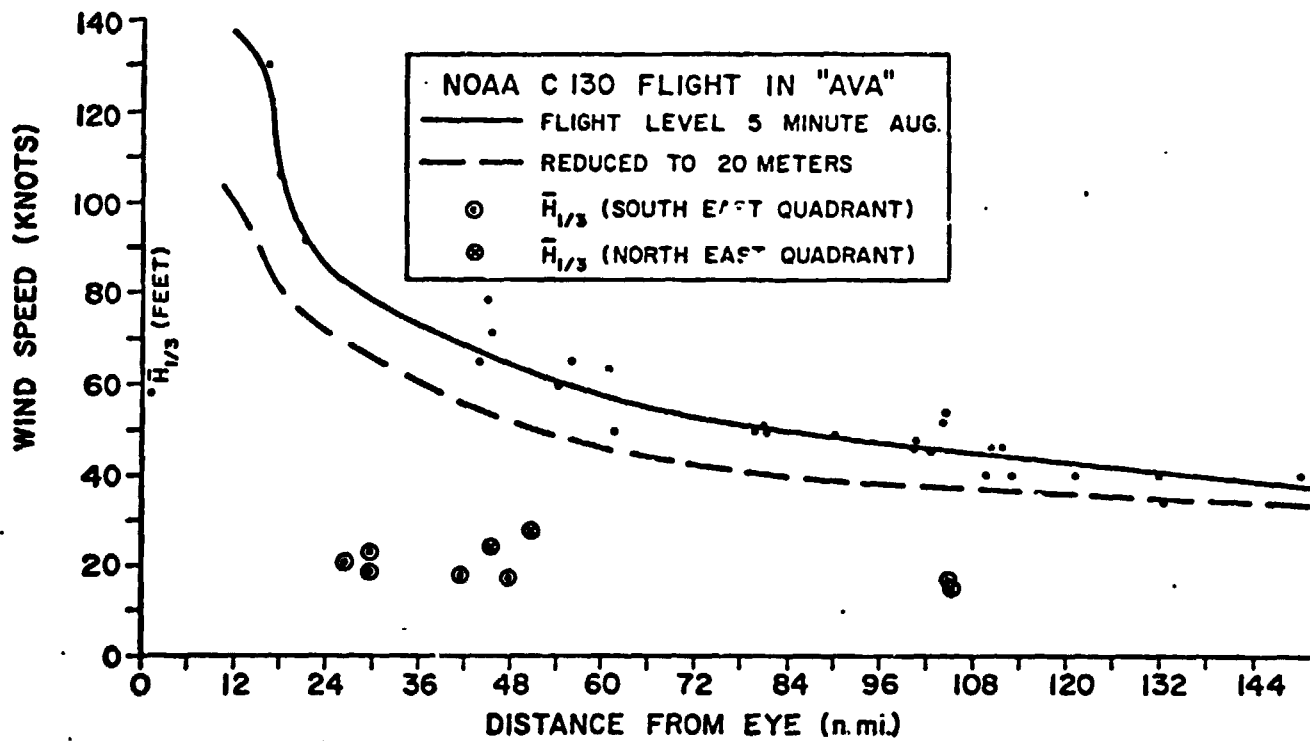
FIGURE 6. RADIAL PROFILE OF WIND SPEED AND SIGNIFICANT WAVE HEIGHT FOR PACIFIC HURRICANE AVA.
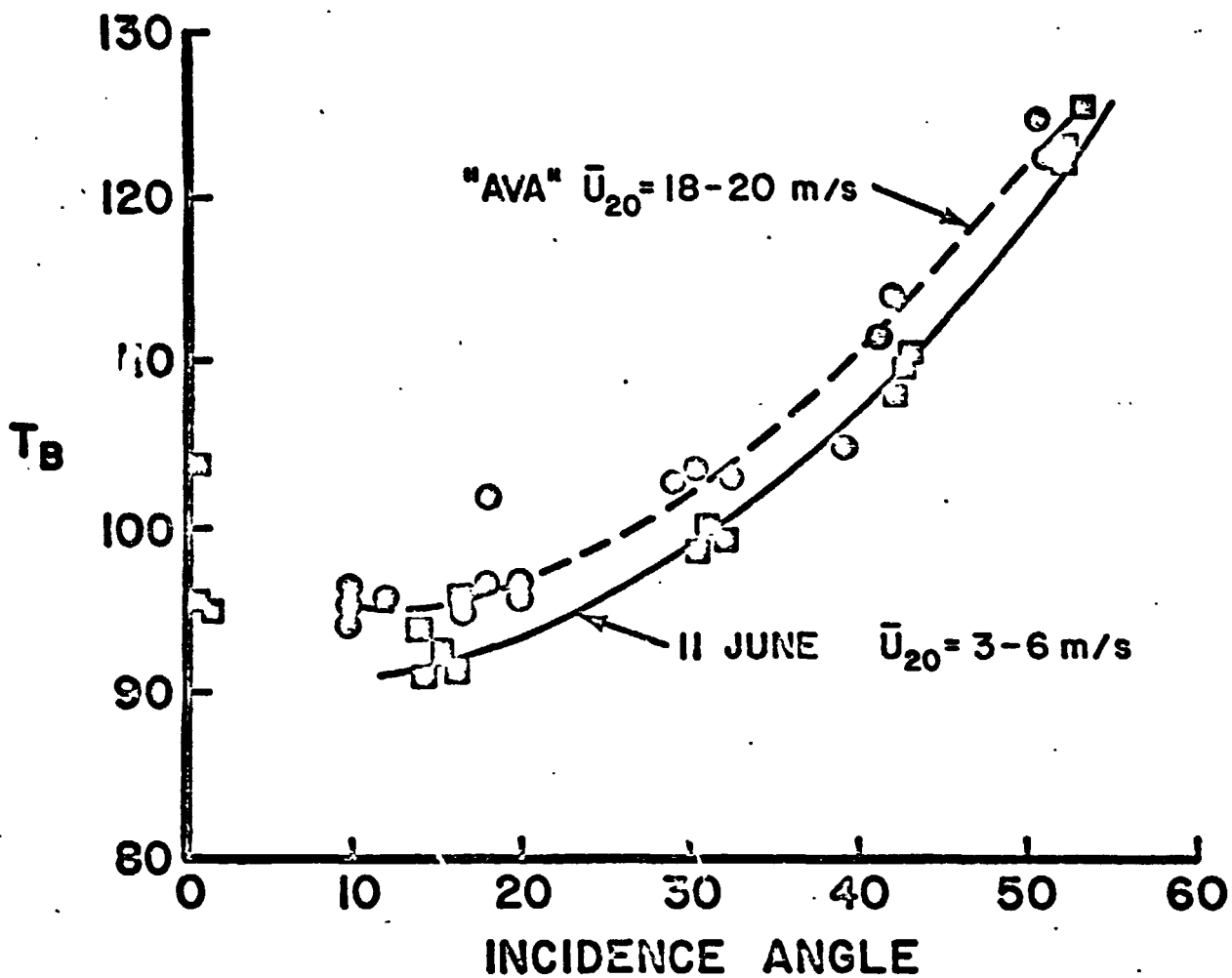
FIGURE 7.   L-BAND VERTICALLY POLARIZED BRIGHTNESS TEMPERATURES
FOR HURRICANE AVA AND LOW WIND CONDITIONS OF 11 JUNE.
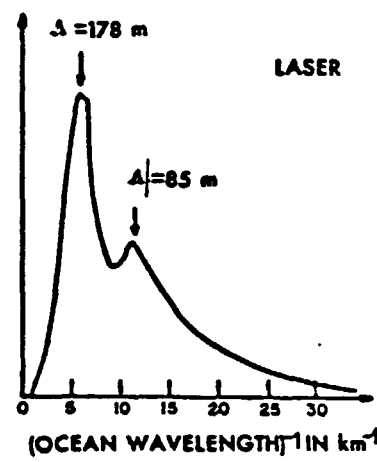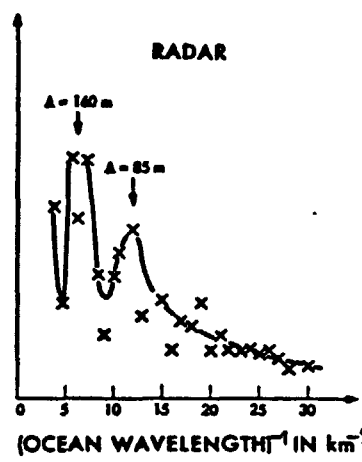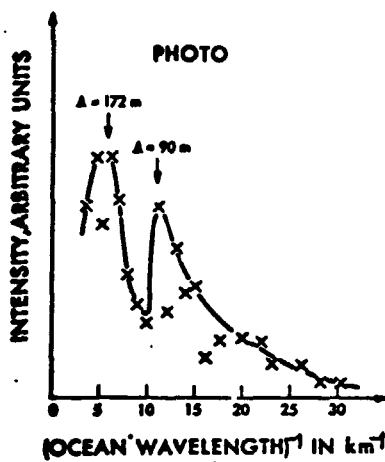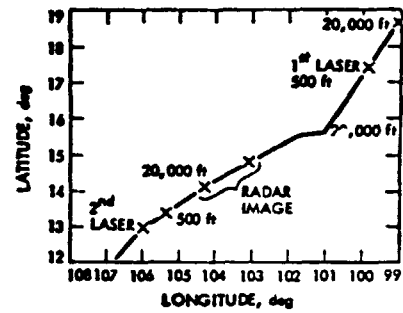
FIGURE 8.   TWO-DIMENSIONAL FOURIER ANALYSIS OF COHERENT RADAR IMAGERY AND
VERTICAL PHOTOGRAPHY OF HURRICANE AVA GENERATED WAVES COMPARED
TO A COMPOSITE OF LASER WAVE MEASUREMENTS AT 13°N, 106°W
AND FOR A FULLY DEVELOPED 11 M/S WIND SPEED.

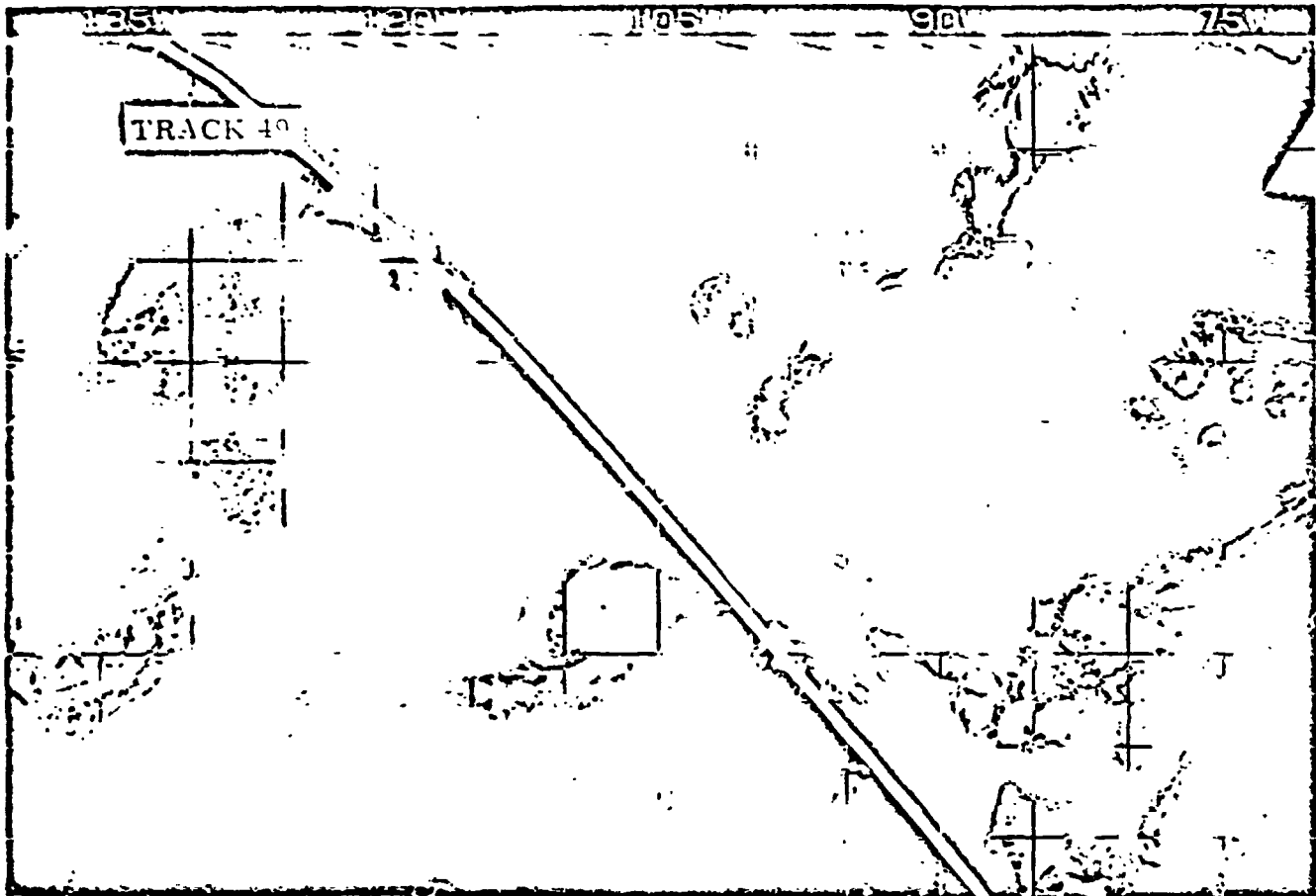**FIGURE 9.** COMPOSITE VIEW OF PACIFIC HURRICANE AVA SHOWING
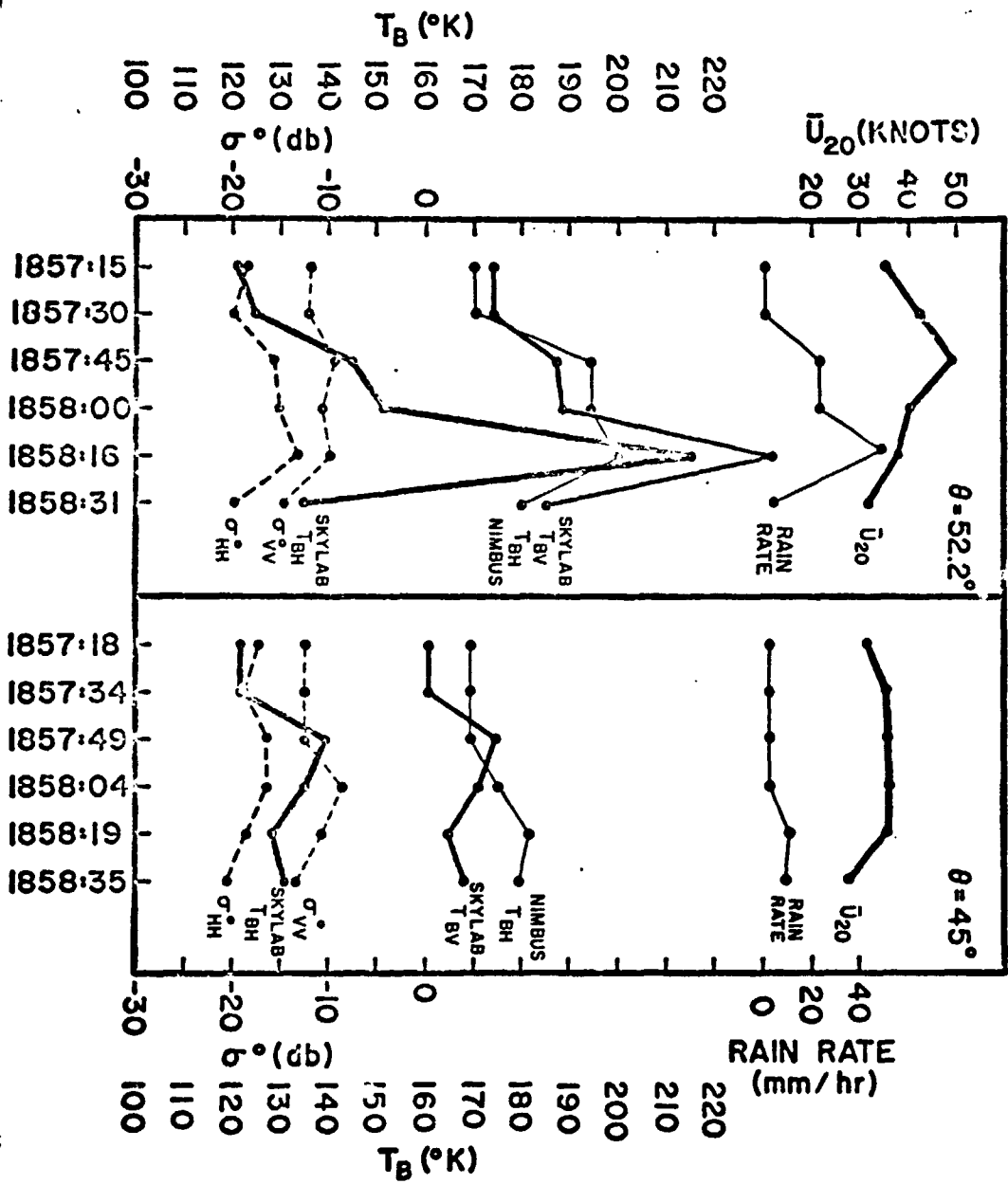PROXIMITY OF THE SKYLAB SUBORBITAL TRACK.

FIGURE 10. ACTIVE AND PASSIVE MICROWAVE OBSERVA-
TIONS OF WIND FIELD IN HURRICANE AVA.